Kelvin−Helmholtz instability in a Hele-Shaw cell

F. Plouraboué
Department of Applied Mathematics and Theoretical Physics, University of Cambridge, Cambridge CB3 9EW, United Kingdom
and Institut de Mécanique des Fluides de Toulouse, Toulouse, 31400, France

E. J. Hinch
Department of Applied Mathematics and Theoretical Physics, University of Cambridge, Cambridge CB3 9EW, United Kingdom

A linear stability analysis is presented for the Kelvin−Helmholtz instability in a Hele-Shaw cell, an analysis based on the Navier−Stokes equation to improve on the previous Euler−Darcy study that Gondret and Rabaud [Phys. Fluids **9**, 3267 (1997)] made of their own experiments.

I. INTRODUCTION

Recently Gondret and Rabaud[1] studied the Kelvin−Helmholtz instability in a Hele-Shaw cell. Two vertical sheets of glass 1.2 m long were held with a 0.35 mm gap separating them. The edges were sealed so as to retain in the lower half a viscous silicon oil and in the upper half nitrogen gas, with a viscosity ratio of a few thousand. Two holes at both ends allowed liquid and gas to be injected at one end at a pressure 10% above atmospheric and removed at the other end, so achieving a horizontal gas flow of several m s^{-1} and in the same direction a liquid flow of several mm s^{-1}. Above a critical flow, the flat interface was unstable and waves grew to a finite amplitude. A small sinusoidal variation in the injection pressure gave a critical flow for different wave numbers. The reduced Reynolds number for the gas flow, appropriate to the nearly unidirectional flow, was about 7 and was very small for the liquid.

In addition to the experiments, Gondret and Rabaud performed a simple stability analysis that successfully predicted the onset of instability. Their analysis adopted the normal description of flow in a Hele-Shaw cell that uses a gap-averaged velocity. To the Darcy equation governing the flow they added the inertia term of Euler, again using only the gap-averaged velocity. Recognizing a little difficulty here in averaging nonlinear terms, Gondret and Rabaud suggested in an Appendix that a correction factor of $\frac{6}{5}$ should multiply the advective derivative, which is appropriate for the average of the product of two velocity fields with parabolic profiles across the gap.

Our purpose in this paper is to replace the gap-averaged description with an asymptotic analysis of the Navier−Stokes equation, exploiting the thinness of the gap compared to the wavelength of the instability, which is of the order of the capillary length $2\pi\sqrt{\gamma/\Delta\rho g}\simeq 1$ cm, with the surface tension γ, density difference $\Delta\rho$, and gravity g. We start in Sec. II with a quick review of the Gondret and Rabaud Euler−Darcy stability analysis, before proceeding to our Navier−Stokes analysis in Sec. III. Both stability analyses are linear. The

results are compared to experiments and discussed in Sec. IV.

II. EULER−DARCY ANALYSIS

If inertia is ignored, the flow in a Hele-Shaw cell is proportional to the pressure gradient in access of the hydrostatic balance,

$$\langle \mathbf{u}\rangle = -\frac{h^2}{3\mu}(\boldsymbol{\nabla} p - \rho \mathbf{g}).$$

Here $\langle \mathbf{u}\rangle$ is the velocity averaged across the gap, $2h$ is the gap thickness, μ the viscosity, p the pressure, ρ the density, and $\mathbf{g}$ the gravitational acceleration. Some inertia can be introduced by first rewriting the Darcy-flow equation as a force balance and then adding the density times the material acceleration of the gap-averaged velocity:

$$\rho\left(\frac{\partial\langle \mathbf{u}\rangle}{\partial t} + \langle \mathbf{u}\rangle\cdot\boldsymbol{\nabla}\langle \mathbf{u}\rangle\right) = -\boldsymbol{\nabla} p + \rho\mathbf{g} - \frac{3\mu}{h^2}\langle \mathbf{u}\rangle. \tag{1}$$

We note that this treatment of the inertial forces is a simplification because some fluid will be moving faster that the gap average and so will have larger accelerations. To take some account of this, Gondret and Rabaud suggested multiplying the $\langle \mathbf{u}\rangle\cdot\boldsymbol{\nabla}\langle \mathbf{u}\rangle$ term by $\frac{6}{5}$, which would be appropriate if the velocity profile across the gap were parabolic. But the profile is not exactly parabolic when inertia forces act differently across the gap, so we will not make their suggested modification.

In the base state, let the gas be in $z>0$ and the liquid in $z<0$. We use subscripts g and l on quantities to denote gas and liquid. The base flow is horizontal with $\mu_g U_g = \mu_l U_l$ because the two flows are driven by the same pressure gradient.

Now consider a small-amplitude perturbation of the interface from $z=0$ to $z=\zeta_0 e^{ik(x-ct)}$, with real positive wave number k and complex wave speed c. We thus start by examining the temporal stability. The small-amplitude approximation requires a small slope $k\zeta_0 \ll 1$. The perturbation flow

is potential, and so has a spatial variation $e^{ik(x-ct)\mp kz}$ in $z \gtrless 0$. Satisfying the kinematic boundary condition, we find the perturbation flow

$$\langle \mathbf{u} \rangle = (\pm 1, i)(U-c)k\zeta_0 e^{ik(x-ct)\mp kz}.$$

The Euler–Darcy momentum equation (1) gives a perturbation pressure,

$$p = \mp \left(\rho(U-c)^2 - i\frac{3\mu}{kh^2}(U-c) \right) k\zeta_0 e^{ik(x-ct)\mp kz}.$$

When imposing the pressure boundary condition, we need to add to the pressure perturbation the basic hydrostatic pressure evaluated at the perturbed surface, $-\rho g\zeta$. The jump in pressure across the boundary is set equal to the capillary pressure $-(\pi/4)\gamma k^2 \zeta$, where we have included the Park and Homsy[2] correction factor $\pi/4$, which takes into account the variation of the principal radii of curvature across the gap for a liquid that is perfectly wetting. Gondret and Rabaud did not include this $\pi/4$ factor. Thus, we obtain the dispersion relation

$$\left(-\rho_g(U_g-c)^2 k + i\frac{3}{h^2}\mu_g(U_g-c) - \rho_g g \right)$$
$$- \left(\rho_l(U_l-c)^2 k - i\frac{3}{h^2}\mu_l(U_l-c) - \rho_l g \right) = -\frac{\pi}{4}\gamma k^2. \quad (2)$$

In the experimental conditions of Gondret and Rabaud of small viscosity and density ratio, $\mu_g \ll \mu_l$ and $\rho_g \ll \rho_l$ with $\rho_g/\rho_l \gg \mu_g^2/\mu_l^2$ so that $\rho_g U_g^2 \gg \rho_l U_l^2$, and small reduced Reynolds number in the liquid flow, $\rho_l U_l k h^2/\mu_l \ll 1$, the dispersion relation (2) reduces to

$$\rho_g U_g^2 k - i\frac{3}{h^2}\mu_l(2U_l-c) - \rho_l g = \frac{\pi}{4}\gamma k^2, \quad (3)$$

where we have used $\mu_g U_g = \mu_l U_l$. From this simplified dispersion relation, we extract the phase velocity c_r and the growth rate kc_i,

$$c_r \simeq 2U_l, \quad kc_i \simeq \frac{k^2 h^2}{3\mu_l} \left(\rho_g U_g^2 - \frac{\rho_l g + \frac{\pi}{4}\gamma k^2}{k} \right). \quad (4)$$

It is useful for later developments to understand the simplified physics in the experimental conditions. Because the liquid is more viscous and has a higher inertia, it moves slowly. The gas thus flows past an effectively stationary liquid surface at $z = \zeta_0 e^{ikx}$. In order to accelerate over the peaks and to decelerate into the troughs of the perturbed interface, there must be a low pressure at the peaks and a high pressure in the troughs. The magnitude of this suction pressure at the peaks is given by Bernoulli as $\rho_g U_g^2 k\zeta_0$. This destabilizing suction is to be offset against the stabilizing effects of the liquid hydrostatic pressure $\rho_l g\zeta_0$ plus a capillary pressure $(\pi/4)\gamma k^2 \zeta_0$. The stabilizing effects win at all wave numbers if the gas velocity is below a critical value: stable if $\rho_g U_g^2 < \sqrt{\rho_l g\pi\gamma}$.

Above the critical gas velocity, there is a range of unstable wave numbers with a net suction pressure at the peaks in the liquid,

$$p_l = \rho_g U_g^2 k\zeta_0 - \rho_l g\zeta_0 - \frac{\pi}{4}\gamma k^2 \zeta_0.$$

The pressure gradient kp_l in the Darcy flow of the liquid induces an upward velocity of the peaks $kc_i\zeta_0 = h^2 kp_l/3\mu_l$, with the result (4) for the growth rate.

The phase velocity of the wave comes from the viscous pressure drop $p_v = 3\mu_g U_g\zeta_0/h^2$ across a peak in the gas flow past the stationary perturbed liquid surface. The pressure gradient kp_v drives a perturbation Darcy flow $h^2 kp_v/3\mu_l = U_l k\zeta_0$ in the liquid, which propagates the interface at U_l relative to the base liquid velocity U_l; hence the result (4) for the phase velocity.

We note that our explanation of the mechanism of the Kelvin–Helmholtz instability in a Hele-Shaw cell is not fraught with the dangers of using Bernoulli suction to explain the original Kelvin–Helmholtz instability between two inviscid fluids. For inviscid fluids, time reversibility implies the existence of two modes, one growing and one decaying, and a correct argument must explain both. Obviously suction at the peak explains the unstable mode. Less obviously, it explains the stable mode. The suction force produces, in an inviscid fluid, an upward acceleration. An upward acceleration of a downward moving peak is a decaying mode.

III. NAVIER–STOKES ANALYSIS

A. Formulation

We now move on from the Gondret and Rabaud Euler–Darcy analysis that used a gap-averaged velocity $\langle \mathbf{u} \rangle$. In this section we calculate the variation of the velocity across the gap using the full Navier–Stokes equation. The linearized Navier–Stokes equation for the perturbation velocity $\mathbf{u}(x,y,z,t)$ and pressure $p(x,y,z,t)$ is

$$\rho \left(\frac{\partial \mathbf{u}}{\partial t} + \mathbf{U}\cdot\nabla\mathbf{u} + \mathbf{u}\cdot\nabla\mathbf{U} \right) = -\nabla p + \mu\nabla^2\mathbf{u}, \quad (5)$$

where the base flow has a parabolic profile across the gap,

$$\mathbf{U} = U\frac{3}{2}\left(1 - \frac{y^2}{h^2} \right)(1,0,0).$$

We again use subscripts g and l for the gas in $z>0$ and liquid in $z<0$.

From our examination of the simplified physics in the experimental conditions of Gondret and Rabaud, we take the gas to flow over an effectively stationary perturbed liquid surface $z = \zeta_0 e^{ikx}$. The wavelength of the instability is much larger than the thickness of the gap. As in lubrication theory and in boundary layer theory, the pressure is asymptotically constant across the thin gap and the pressure-driven gas flow is in the plane of the walls. In these circumstances, we find that a possible solution of the linearized Navier–Stokes equation (5) is a potential pressure field,

$$p = \rho_g U_g^2 k\zeta_0 e^{ikx-kz}P,$$

with nondimensional pressure amplitude P, along with a flow in the direction of the pressure gradient,

$$\mathbf{u} = (1,0,i)U_g k\zeta_0 e^{ikx-kz}f(y/h),$$

with a variation across the gap given by the nondimensional profile f. We define the nondimensional coordinate across the gap $\eta = y/h$. The above ansatz for the pressure and velocity satisfy the linearized Navier–Stokes equation (5) if the velocity profile f and pressure amplitude P satisfy

$$\tfrac{3}{2}(1-\eta^2)f = -P + \frac{1}{i\,\mathrm{Re}}f'', \tag{6}$$

with reduced Reynolds number $\mathrm{Re} = \rho_g U_g k h^2/\mu_g$ for the gas flow. The no-slip boundary condition on the sidewalls is

$$f = 0, \quad \text{at } \eta = \pm 1.$$

The kinematic boundary condition on the effectively stationary liquid surface does not match the velocity profile f. Realizing that there will be an adjustment zone near the meniscus with a height equal to the width of the gap, we need only require the total normal component of the mass-flows match. Hence we normalize the solution to have net flow of unity in the nondimensionalization,

$$\int_0^1 f\,d\eta = 1.$$

The dynamic boundary condition equates the capillary pressure to the jump between the pressure in the Darcy flow of the liquid, including a liquid hydrostatic contribution at the perturbed surface, and the dynamic gas pressure described by the pressure amplitude P,

$$\rho_g U_g^2 k P + i\frac{3\mu_l}{h^2}(U_l - c) + \rho_l g = -\frac{\pi}{4}\gamma k^2,$$

corresponding to the simplified dispersion relation (3) in the Euler–Darcy analysis. Solving for the phase velocity c_r and the growth rate $k c_i$, we find

$$c_r = U_l(1 + \tfrac{1}{3}\mathrm{Re}P_i,) \quad k c_i = \frac{k^2 h^2}{3\mu_l}\left(-\rho_g U_g^2 P_r - \frac{\rho_l g + \frac{\pi}{4}\gamma k^2}{k}\right), \tag{7}$$

where $P = P_r + iP_i$ and where we have used $\mu_l U_l = \mu_g U_g$ to simplify the phase velocity.

B. Numerical solution

The velocity profile f was found by integrating Eq. (6) numerically with a fourth-order Runge–Kutta scheme. A solution was first found to the non-normalized problem, setting $P = 1$ and shooting from $\eta = 0$ with symmetric condition $f'(0) = 0$ and a guess for the complex value of $f(0)$ that was adjusted by linear extrapolation to give $f(1) = 0$. The solution pair f and P were then both divided by $\int_0^1 f\,d\eta$ in order to normalize the solution.

Results for the velocity profile $f(\eta)$ at Reynolds numbers $\mathrm{Re} = 1, 3, 10, 30, 100$ are given in Fig. 1. The real and imaginary parts are plotted separately. At low Reynolds numbers, $\mathrm{Re} \leqslant 3$, the velocity profile is parabolic and mostly real. At high Reynolds numbers, $\mathrm{Re} \geqslant 30$, the velocity decreases in the center of the gap and peaks near the walls.

Results for the pressure amplitude P as a function of the Reynolds number Re are given in Fig. 2. At low Reynolds

numbers, the pressure amplitude varies as $P \sim 3i/\mathrm{Re}$. At high Reynolds numbers, the pressure amplitude is complex and decreases.

C. Low Reynolds numbers

The low Reynolds number behavior can be studied by making an asymptotic expansion,

$$f \sim f_0 + \mathrm{Re}\,f_1,$$
$$P \sim \mathrm{Re}^{-1}P_0 + P_1.$$

The governing equation (6), boundary conditions, and normalization are all expanded. At leading order we find the Poiseuille profile of inertialess Darcy flow,

$$f_0 = \tfrac{3}{2}(1-\eta^2), \quad P_0 = 3i.$$

The inertia-induced correction is

$$f_1 = i\,\tfrac{3}{280}(-5 + 33\eta^2 - 35\eta^4 + 7\eta^6), \quad P_1 = -\tfrac{54}{35}.$$

The numerical results in Fig. 1 for the velocity profile $f(\eta)$ are consistent with these asymptotic results. At Reynolds numbers 1 and 3, the real part is parabolic in shape with a centreline value of 1.5. The imaginary part, with vanishing integral from the normalization constraint, is positive near the walls and negative in the center, with a centerline value of $-0.054\,\mathrm{Re}$. Figure 2 for the pressure amplitude also exhibits the asymptotic behavior of $P_i \sim 3/\mathrm{Re}$ and $P_r \sim -\tfrac{54}{35} = -1.543$.

At low Reynolds numbers we have found the pressure amplitude from the Navier–Stokes equation is

$$P \sim 3i\,\mathrm{Re}^{-1} - \tfrac{54}{35}. \tag{8}$$

The corresponding nondimensional expression from the Euler–Darcy analysis of Sec. II, valid for all Reynolds numbers, is

$$P \sim 3i\,\mathrm{Re}^{-1} - 1.$$

Thus, the destabilizing inertial effects, the real part of P, are more than 50% larger than estimated by the Euler–Darcy approximation. The Gondret and Rabaud correction factor of $\tfrac{6}{5}$ is seen to be insufficient, at least at low Reynolds numbers.

We have already noted that the value of the Reynolds number in the experiments for the flow of gas was 7. The numerical results in Fig. 2 show that the low Reynolds number asymptotics will provide a reasonable estimate for the pressure amplitude at this less-than-small value, to within errors of 15%.

D. High Reynolds numbers

At high Reynolds numbers, the gas flow has a different behavior in the center of the gap and near the walls. In the center, the pressure perturbation accelerates the gas as it is advected along by the mean flow,

$$f \sim -P/\tfrac{3}{2}(1-\eta^2).$$

Thus, the velocity profile increases away from the centerline; see Fig. 1 for $\mathrm{Re} = 30$ and 100, because moving with slower mean flow off the centerline it has longer to be accelerated.
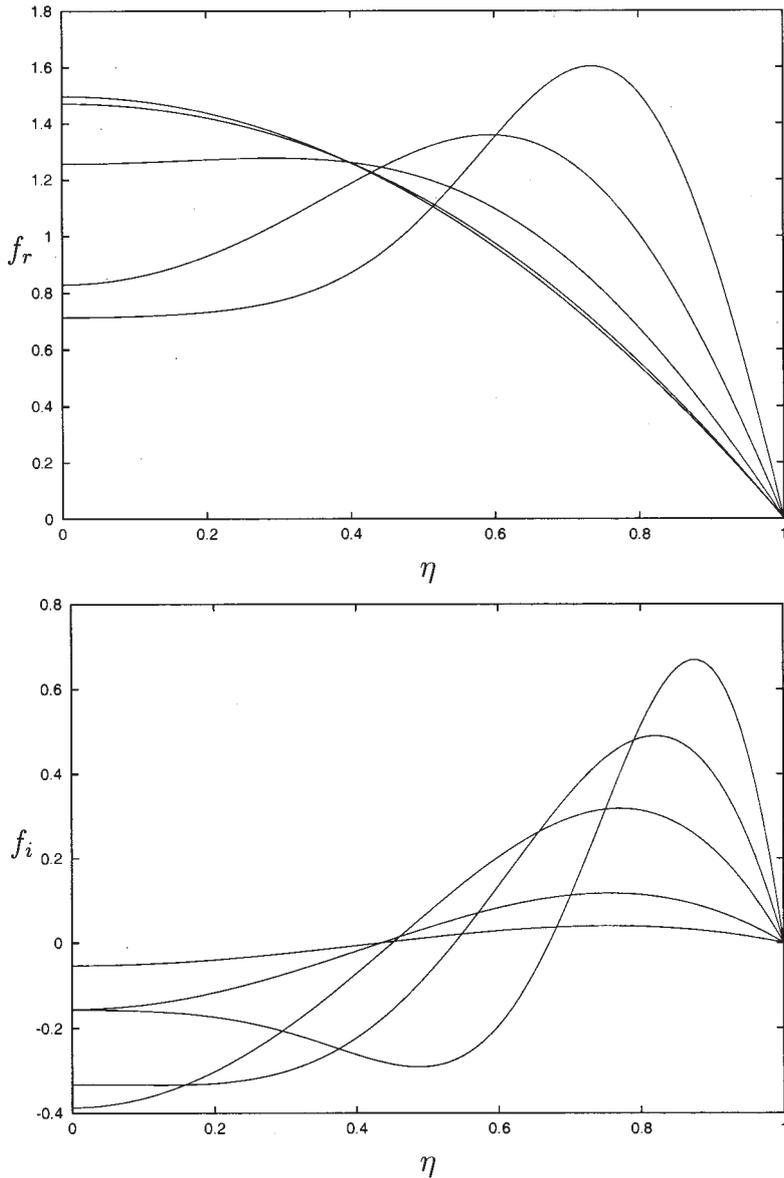
FIG. 1. The velocity profiles $f(\eta)$ at various Reynolds numbers, Re=1, 3, 10, 30, and 100. In the real part f_r, the centerline value $f_r(0)$ decreases as the Reynolds number increases. The value of the imaginary part near the wall $\eta=1$ increases as the Reynolds number increases.

Near the walls viscosity becomes important. A balance between viscosity and advection is possible within a boundary layer of thickness $\delta=\mathrm{Re}^{-1/3}$, where to match with the interior $f=O(P/\delta)$. To exhibit this boundary layer behavior, we have plotted in Fig. 3, $f_r\delta/P$ as a function of $(1-\eta)/\delta$, at Re=30, 100, 300, and 1000. We see that with this rescaling the peaks in the velocity occur at the same position in the boundary layer and with essentially the same amplitude.

The normalization integral has a leading-order contribution $\int_0^{1-\delta}P/3(1-\eta)d\eta \sim \frac{1}{3}P\ln\delta$, along with $O(1)$ corrections from the boundary layer and the central region. We have evaluated these $O(1)$ contributions numerically as

$$\int_0^1 f\,d\eta \sim -P(\tfrac{1}{9}\ln\mathrm{Re}+0.402+i0.175).$$

Equating this to unity gives the asymptotic behavior of the pressure amplitude at large Reynolds numbers,

$$P \sim -1/(\tfrac{1}{9}\ln\mathrm{Re}+0.402+i0.175). \qquad (9)$$

These asymptotic results are plotted in Fig. 2.

At high Reynolds numbers the pressure amplitude P decreases slowly with increasing Reynolds number. This decrease has its origin in the slow speed of the base flow near to the walls. Taking longer to be advected at this slow speed through a wavelength, a smaller pressure perturbation is required to achieve the same velocity perturbation. The consequences of the smaller pressure amplitude P in dispersion relation (7) are a smaller phase velocity and lower growth rate: it is as if the base flow is moving slower. Thus at high Reynolds numbers the instability is controlled not by the gap-averaged value of the base velocity nor the average of its square, giving greater weight to the peaks and leading to the Gondret and Rabaud suggested factor of $\frac{6}{5}$, but is more influenced by the slower moving parts of the base flow.
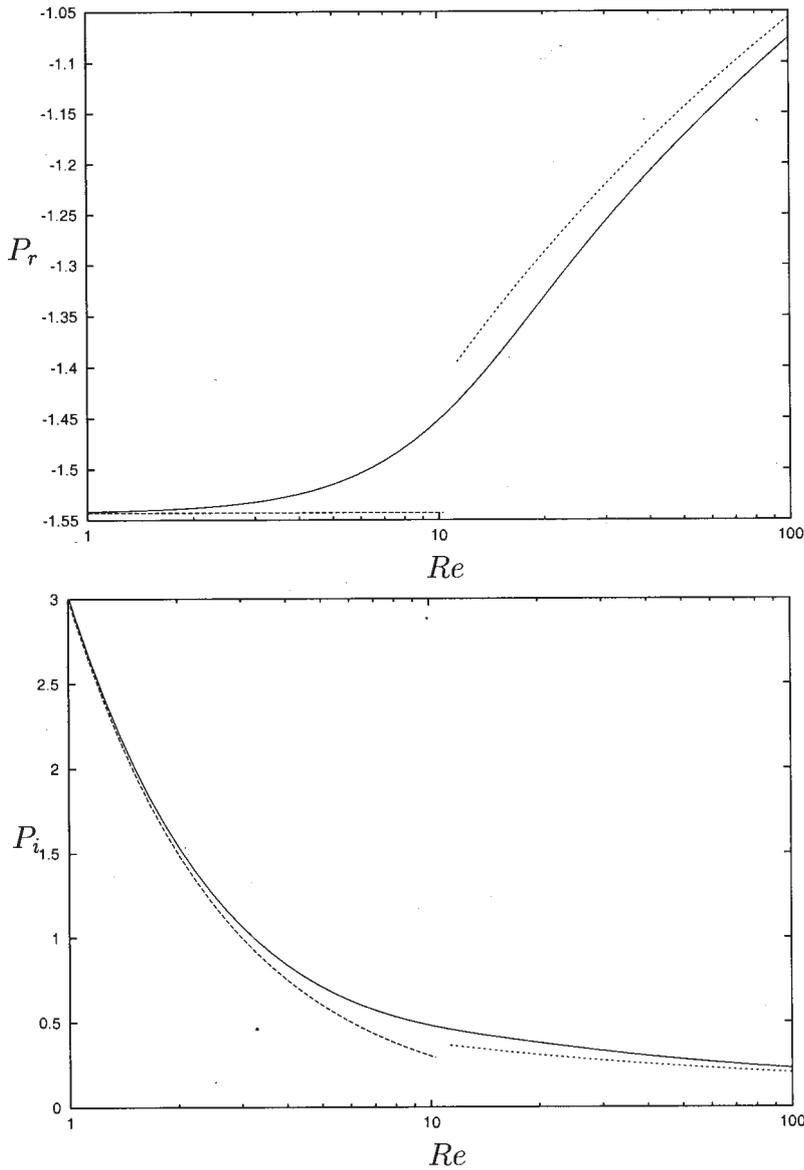
FIG. 2. The pressure amplitude P as a function of the Reynolds number Re. The dashed curves are the small Reynolds number asymptotic result (8), while the dotted curves are the high Reynolds number result (9).

IV. COMPARISON WITH EXPERIMENTS

A. Threshold of instability

In this section we compare our theoretical predictions with the experimental observations of Gondret and Rabaud.[1] We start with the minimal gas velocity for the appearance of the instability, and in the following section look at the phase velocity.

In their experiments, Gondret and Rabaud added a small oscillatory perturbation to the pressure of the liquid as it entered the device. Varying the frequency of this excitation, they could measure the threshold velocity of the gas for instability at different observed wave numbers. A more careful measurement of the decay length of stable waves suggested that the true critical velocity might be 2% higher than these reported threshold velocities. We plot in Fig. 4 their threshold gas velocities U_g has a function of the observed wave number k. We have nondimensionalized these observed quantities using the natural capillary length l_* and the gas velocity V_* whose Bernoulli pressure has the capillary pressure of this length,

$$l_* = \sqrt{\frac{\pi \gamma}{4 \rho_l g}} \quad \text{and} \quad V_* = \sqrt{\frac{\pi \gamma}{2 \rho_g l_*}}.$$

In the experiments, $\gamma = 2.06\ 10^{-2}\ \mathrm{N\,m^{-1}}$, $\rho_l = 965\ \mathrm{kg\,m^{-3}}$, $g = 9.81\ \mathrm{m\,s^{-2}}$, and $\rho_g = 1.28\ \mathrm{kg\,m^{-3}}$, so that $l_* = 1.31 \times 10^{-3}$ m and $V_* = 4.40\ \mathrm{m\,s^{-1}}$.

Using these scalings, the predictions of the Euler–Darcy analysis of Sec. II for the threshold gas velocity may be written as

$$\left(\frac{U_g}{V_*}\right)^2 = \frac{1 + (kl_*)^2}{2kl_*}, \tag{10}$$

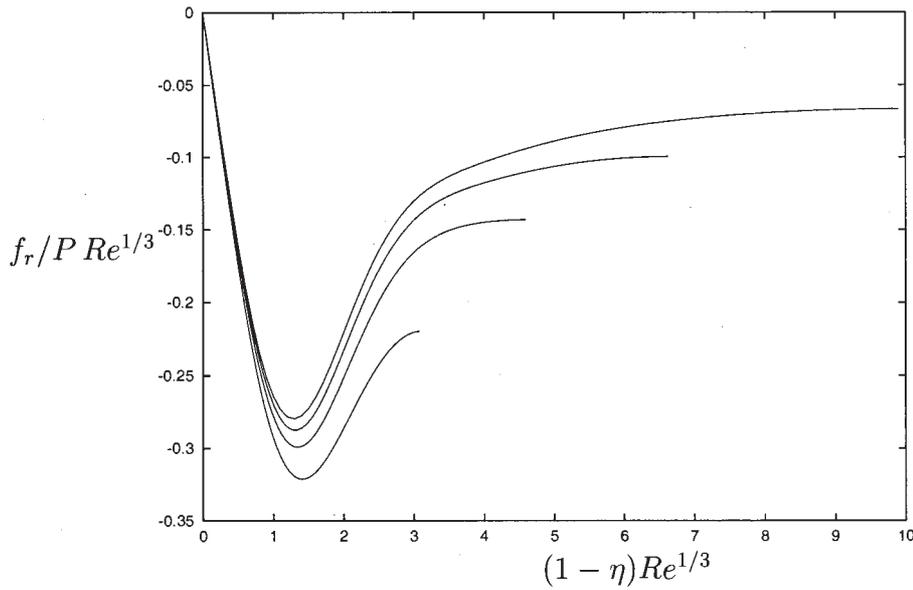which is also plotted in Fig. 4, along with our results from the Navier–Stokes analysis of Sec. III,

FIG. 3. The boundary layer scaling of the velocity profile at high Reynolds numbers. The curves increasing from the bottom are for Reynolds number Re=30, 100, 300, and 1000.

$$\left(\frac{U_g}{V_*}\right)^2 = \frac{1+(kl_*)^2}{2kl_*}\frac{1}{-P_r(\mathrm{Re})}, \tag{11}$$

where P_r is the real part of the pressure amplitude. It is a function of the reduced Reynolds number $\mathrm{Re}=U_g kh^2/\nu$, see Fig. 2, and so varies with the gas velocity U_g and the wave number k. In the range of interest, $P_r \approx -1.5$. Being larger than unity, the Navier–Stokes analysis predicts a lower critical gas velocity, lower by about $1/\sqrt{1.5}$, i.e., about 82% of the Euler–Darcy value.

Figure 4 shows that the improved Navier–Stokes theory does not produce improved predictions of the experimental results. In view of these poor predictions, we have considered a number of differences between our theory and the experimental conditions. First we have assumed that the vis-

cosity and the density of the liquid are very much larger than the values of the gas, so that the liquid appears to be stationary as far as the gas flow is concern. It is not difficult to generalize our approach to the Navier–Stokes problem to the case of two fluids with arbitrary viscosity and density ratios. We find that if the experiments had used air and water then there would have been a 5% overestimate by the assumption of infinity ratios. The experiments, however, used a much more viscous liquid, and for this larger ratio we find that there would be no detectable change in Fig. 4.

Another simplification of our theory is the assumption that the gas flow is incompressible. With gas velocities a few percent the speed of sound, one would anticipate modifications of the gasdynamics by the square of that ratio, i.e.,
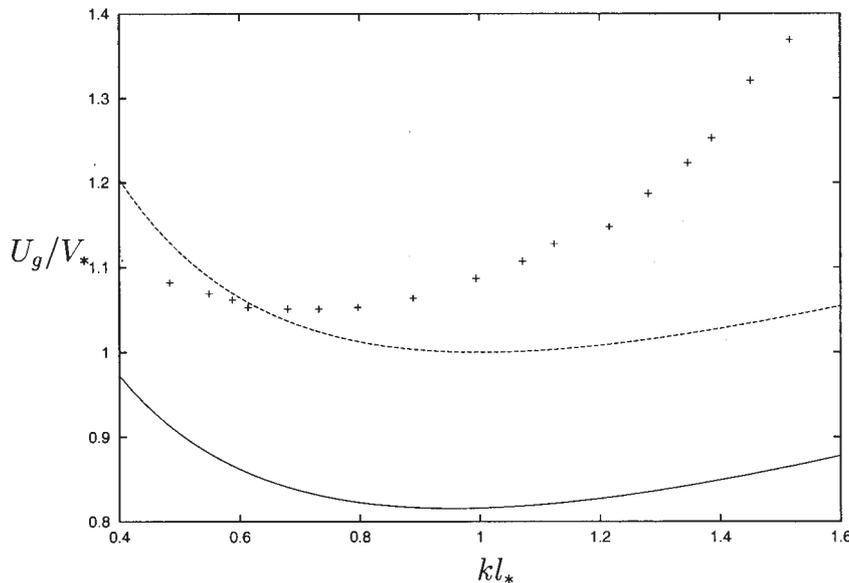

FIG. 4. The critical velocity of the gas U_g for the appearance of an instability as a function of the wave number k, nondimensionalized by the capillary length l_* and the associated gas velocity V_*. The points are the experimental results of Gondret and Rabaud. The dashed curve is the prediction (10) of the Euler–Darcy analysis, while the continuous curve is the prediction (11) of the Navier–Stokes analysis.

totally negligible. There is, however, an effect of the compressibility on the base state of the gas, because the inlet pressure was typically 10% above the atmospheric pressure. This means that the density of the gas near the inlet is typically 10% higher. This in turn reduces the value of our velocity scale V_* by 5%. The experimental conditions near to the inlet are relevant, because it is there that one observes whether the waves are growing or decaying.

The 10% increase in the base pressure near the inlet has a second effect. The gas velocity was measured in the experiments by applying Darcy's law to the basic pressure gradient, which was assumed to be linear and given by the difference between the pressure at the inlet and outlet divided by the distance between them. A linear pressure gradient gives a gas velocity that is constant along the channel. A constant gas velocity does not give a constant mass flux when the density varies. In order to have a constant mass flux, the square of the pressure must vary linearly down the channel. This means that the gas velocities are 5% lower near the inlet and 5% higher near the outlet. Hence one should reduce the observed gas velocity U_g by 5%. As the velocity scale V_* should also be reduced by 5%, there will be no effect on the plotted ratio U_g/V_*. The fact that the ratio U_g/V_* does not change value is an unforeseen advantage of making the nondimensional plot.

Our theoretical study also assumed that the base flow was horizontal, i.e., we ignored the radial flow out of the source and into the sink at the ends of the channel. This radial flow introduces an extra pressure drop, roughly equivalent to extending the length of the channel for each hole by $(H/2\pi)\ln(H/2\pi R)$, where H is the height of the gas flow and R is the radius of of the hole. In the experiments $H=5$ cm and $R=3.5$ mm, so we find that each hole adds 6.5 mm to the length of the 1.2 m channel, i.e., a correction of just over 1%. As the experimental velocities were calculated from an assumed Darcy flow, this 1% extra pressure drop reduced the observed velocities by 1%, which is in the correct direction but too small in magnitude. We have not adjusted the experimental data for this small effect.

A further assumption in our theory that affects the threshold velocity is the assumption that the basic flow has a parabolic profile. At the reduced Reynolds number of Re $=7$, the base flow only becomes fully established after one wavelength, i.e., about 1 cm. We note, however, that in the experiments a splitter plate of 10 cm divides the streams of gas and liquid before they meet. Hence, at the separation of the plates and at the velocities used, the base flow should be fully established at the place where the instability was observed.

Finally, our analysis made a long wave approximation, $kh \ll 1$. This resulted in the neglect of the slightly different flows near the meniscus, modifications of the flow that extend away from the meniscus a distance of about a gap thickness. In the experiments the value of this small parameter was $kh=0.13$, which may not be so small. We are currently trying to develop a theory for this correction, but at this time we have no estimate of the magnitude of the correction.

B. Phase velocity

The phase velocity was measured by Gondret and Rabaud[1] to be $c_r=1$ mm s^{-1}. We discuss the phase velocity in a nondimensionalized form by scaling with the velocity of the liquid when the gas has the velocity V_*, i.e., scaled with $V_{l*} = \mu_g V_*/\mu_l$. In the experiments, $V_*=4.4$ m s^{-1}, $\mu_g = 1.75 \times 10^{-5}$ Pa s and $\mu_l = 0.1$ Pa s, so that $V_{l*} = 0.77$ mm s^{-1}. Thus, the nondimensional measure of the observed velocity is $c_r/V_{l*}=1.30$.

The Euler–Darcy theory of Sec. II predicts a phase velocity that is a little higher, $c_r/U_l=2.00$, i.e., $c_r/V_{l*} = 2.00$. The Navier–Stokes analysis of Sec. III predicts at the Reynolds number Re$=5.84$, corresponding to the marginal waves with $U_g/V_* = 0.816$ and $kl_* = 0.95$, a pressure amplitude $P_i = 0.637$, which gives a phase velocity by (7), $c_r/U_l = 2.24$, i.e., $c_r/V_{l*}=1.83$. The two theories thus significantly overestimate the phase velocity of the marginally stable waves. The omissions of the theories discussed in the previous section would obviously lead to some minor adjustments to these values, but would not give the significant correction required.

One feature of the our simplified treatment of the meniscus does, however, have a significant effect on the phase velocity without modifying the gas velocity at the threshold of the instability. The two theories apply a pressure condition at the interface with a jump of the capillary pressure $(-\pi/4)\gamma k^2 \zeta$. This takes into account the curvature of the interface in the xz plane. There is, however, a much larger curvature $1/h$ in the perpendicular y direction across the gap. The large capillary pressure γ/h associated with this curvature does not alter the analysis because it is constant, independent of the displacement of the interface. A problem arises, however, from relatively small corrections to this large constant pressure jump, because the corrections can be of the same size as the term $(-\pi/4)\gamma k^2 \zeta$, and they can also vary with the displacement of the interface.

The liquid used in the experiments wets the sidewalls perfectly, and so to leading order the meniscus adopts a semicircular shape across the gap. As the wave crests propagate along the channel, the meniscus rises and falls. As the meniscus falls it leaves a thin film on the sidewalls of thickness $1.34h(\mu_l u_n/\gamma)^{2/3}$, where u_n is the normal velocity of the interface. The presence of these thin films increases slightly the curvature of the interface, contributing to a slightly higher jump in the capillary pressure. Viscous dissipation in the thin films leads to a similar additional contribution to the pressure drop. This problem was studied by Bretherton.[3] Adopting his results for a tube to our channel, he found the pressure drop across the falling meniscus is

$$\frac{\gamma}{h}\left[1 + 3.723\left(\frac{\mu_l u_n}{\gamma}\right)^{2/3}\right],$$

and the pressure drop across a meniscus rising over a film left behind by the meniscus descending at the same speed,

$$\frac{\gamma}{h}\left[1 - 0.976\left(\frac{\mu_l u_n}{\gamma}\right)^{2/3}\right].$$

The difference between these two pressures must be added to our jump in the capillary pressure $(-\pi/4)\gamma k^2 \zeta$.

Now for the marginally stable surface displacement $\zeta = \zeta_0 \cos k(x-c_r t)$, the normal velocity of the interface is $u_n = \zeta_0 k c_r \sin k(x-c_r t)$, i.e., out of phase with the displacement. To use in the linear stability analysis the new additional pressure drop, which is nonlinear, we break $\sin^{2/3}$ into its Fourier components, in particular, $\sin^{2/3} = 1.0712 \sin + $ higher harmonics. Adding the extra out-of-phase pressure jump to the boundary condition, we find that the expression for the phase velocity (7) becomes

$$\frac{c_r}{U_l} = 1 + \tfrac{1}{3} \operatorname{Re} \mathrm{P}i$$

$$- 1.67 \left(\frac{\mu_l U_l}{\gamma} \right)^{-1/3} (kh)^{2/3} \left(\frac{h}{\zeta_0} \right)^{1/3} \left(\frac{c_r}{U_l} \right)^{2/3}.$$

The expression for the growth rate is unaffected, because it uses the component of the pressure in phase with the surface displacement, or, in more physical terms, the destabilizing Bernoulli suction only sees a stationary liquid surface.

Applying our new expression for the phase velocity to the experiments, we take $U_l = 0.63 \text{ mm s}^{-1}$, so that the capillary number $\mu_l U_l / \gamma = 3.0 \times 10^{-3}$. We do not know the amplitude of the observed waves, but looking at the figures in Gondret and Rabaud,[1] we take $\zeta_0 = 1$ mm. The equation for the phase velocity then becomes

$$\frac{c_r}{U_l} + 1.63 \left(\frac{c_r}{U_l} \right)^{2/3} = 2.23,$$

with solution $c_r/U_l = 0.82$, i.e., $c_r/V_{l*} = 0.67$. This value is much smaller than the observed value, whereas the original theory gave much larger. While there are considerable uncer-
tainties in our analysis in this section, for example, our selection of the amplitude of the wave, it is clear that the effect is significant. Some additional experiments could usefully be made measuring the pressure jump across a meniscus in a Hele-Shaw cell that oscillates up and down with similar amplitudes to those of the propagating waves.

After their first paper on the subject, Gondret, Ern, Meignin, and Rabaud[4] went on to study the transition from convective instability to absolute instability by following the evolution of an initial impulse. They found the transition to absolute instability occurred in their experiments when the gas velocity was 15% higher than the threshold for any instability. A numerical study of the Euler–Darcy dispersion relation, now including the $\pi/4$ Park and Homsy factor and a factor of $\tfrac{6}{5}$ multiplying the nonlinear terms, predicted the transition to absolute instability occurred 7% above the threshold for any instability. We have repeated their analysis for our Navier–Stokes dispersion relation and find that its transition occurs at 22% above threshold. We can now note that these calculations of the transitions to absolute instability involve the out-of-phase pressure term P_i and so would be modified significantly by including Bretherton's extra pressure jump. Further, the nonlinear dependence of the extra pressure jump is not the normal quadratic dependence.

[1]P. Gondret and M. Rabaud, "Shear instability of two-fluid parallel flow in a Hele-Shaw cell," Phys. Fluids **9**, 3267 (1997).
[2]C.-W. Park and G. M. Homsy, "Two-phase displacement in Hele Shaw cells: Theory," J. Fluid Mech. **139**, 291 (1984).
[3]F. P. Bretherton, "The motion of long bubbles in tubes," J. Fluid Mech. **10**, 166 (1961).
[4]P. Gondret, P. Ern, L. Meignin, and M. Rabaud, "Experimental evidence of a nonlinear transition from convective to absolute instability," Phys. Rev. Lett. **82**, 1442 (1999).